CERN – EUROPEAN ORGANIZATION FOR NUCLEAR RESEARCH

CLIC – Note – 1083

NATURAL SOURCES OF GEOMAGNETIC FIELD VARIATIONS

Balázs Heilig[1], Ciarán Beggan[2], János Lichtenberger[3]

[1]Mining and Geological Survey of Hungary, Tihany, Hungary
[2]British Geological Survey, United Kingdom
[3]Eötvös University, Budapest, Hungary

CERN-ACC-2018-0033
10/10/2018

Abstract

The Earth's magnetic field is a dynamic system and varies on a wide spectrum of timescales from microseconds to hundreds of millions of years.
The primary source of the field is the self-sustaining geodynamo action of the Earth's liquid outer core. This creates around 95% of the magnetic field strength at the Earth's surface. Its average strength at mid-latitudes is on the order of 50,000 nT (ranging between 20,000-60,000 nT increasing toward the poles). The core field varies on timescales of years to millennia. Another internal source is the quasi-stable crustal field, generated by the heterogeneous distribution of ferromagnetic minerals in the upper 5-30 km of the Earth's surface. Its contribution is much smaller at around 20 nT on average globally, though it can locally be much larger. It changes on timescales of millions of years except at sources such as active volcanic regions or along mid-ocean ridges.
There are a number of external (i.e. with sources outside the Earth) field systems which are created by solar-terrestrial interactions. These are much more dynamic and vary on timescales of seconds to days. These have magnitudes of a few pT to 100 nT on geomagnetically quiet days but can change rapidly within minutes to thousands of nT, for example from the impact of an Interplanetary Coronal Mass Ejection upon the Earth. These effects (geomagnetic storms and substorms) are strongly dependent on local time and latitude, with high latitudes (|Φgeomagnetic|

> 60°) being particularly affected from the auroral electrojet current systems or magnetospheric waves. Due to simple geometric reasons (zonal currents), most of the above geomagnetic disturbances appear in the geomagnetic north (also called the horizontal) component. Other magnetic fields are generated locally by instantaneous phenomena such as lightning-generated spherics and magnetospheric whistlers.

We will briefly outline the spatio-temporal variation and largest dynamic expected from each source. In this concise review we focus on mid-latitudes (CERN is located at 46.2° geographic latitude, 40.4° geomagnetic latitude, at the footpoint of the L=1.8 magnetic McIlwain-shell) and neglect some of the high-latitude/auroral and equatorial phenomena not relevant for CERN's location.

Geneva, Switzerland
10 October 2018

Natural sources of geomagnetic field variations

Heilig, Balázs, Mining and Geological Survey of Hungary, Tihany, Hungary
Beggan, Ciarán, British Geological Survey, United Kingdom
Lichtenberger, János, Eötvös University, Budapest, Hungary

Introduction

The Earth's magnetic field is a dynamic system and varies on a wide spectrum of timescales from microseconds to hundreds of millions of years.

The primary source of the field is the self-sustaining geodynamo action of the Earth's liquid outer core. This creates around 95% of the magnetic field strength at the Earth's surface. Its average strength at mid-latitudes is on the order of 50,000 nT (ranging between 20,000-60,000 nT increasing toward the poles). The core field varies on timescales of years to millennia. Another internal source is the quasi-stable crustal field, generated by the heterogeneous distribution of ferromagnetic minerals in the upper 5-30 km of the Earth's surface. Its contribution is much smaller at around 20 nT on average globally, though it can locally be much larger. It changes on timescales of millions of years except at sources such as active volcanic regions or along mid-ocean ridges.

There are a number of external (i.e. with sources outside the Earth) field systems which are created by solar-terrestrial interactions. These are much more dynamic and vary on timescales of seconds to days. These have magnitudes of a few pT to 100 nT on geomagnetically quiet days but can change rapidly within minutes to thousands of nT, for example from the impact of an Interplanetary Coronal Mass Ejection upon the Earth. These effects (geomagnetic storms and substorms) are strongly dependent on local time and latitude, with high latitudes ($|\Phi_{geomagnetic}| > 60°$) being particularly affected from the auroral electrojet current systems or magnetospheric waves. Due to simple geometric reasons (zonal currents), most of the above geomagnetic disturbances appear in the geomagnetic north (also called the horizontal) component. Other magnetic fields are generated locally by instantaneous phenomena such as lightning-generated spherics and magnetospheric whistlers.

We will briefly outline the spatio-temporal variation and largest dynamic expected from each source. In this concise review we focus on mid-latitudes (CERN is located at 46.2° geographic latitude, 40.4° geomagnetic latitude, at the footpoint of the L=1.8 magnetic McIlwain-shell) and neglect some of the high-latitude/auroral and equatorial phenomena not relevant for CERN's location.

Contributions from magnetospheric-ionospheric current systems

We first consider the sources related the magnetosphere-ionosphere system, which is largely driven directly or indirectly by the Sun or its magnetic field interaction through the solar wind.

Sq – Solar quiet variation. The Solar quiet ionospheric current system takes place at around 110 km altitude in the upper atmosphere, where solar EUV and X-ray radiation ionizes the molecules into electrons and ions. These charged particles are pushed by Sun-driven neutral winds across the Earth's magnetic field to form a dynamo. The related current system consists of two counter-

streaming hemispherical cells which follow the sub-solar point around the globe. The ground magnetic effect has a range of around 50 nT at mid-latitude, largest at the latitude of the cells' foci, and has a regular diurnal variation. The amplitude has a strong seasonal and solar cycle dependence.

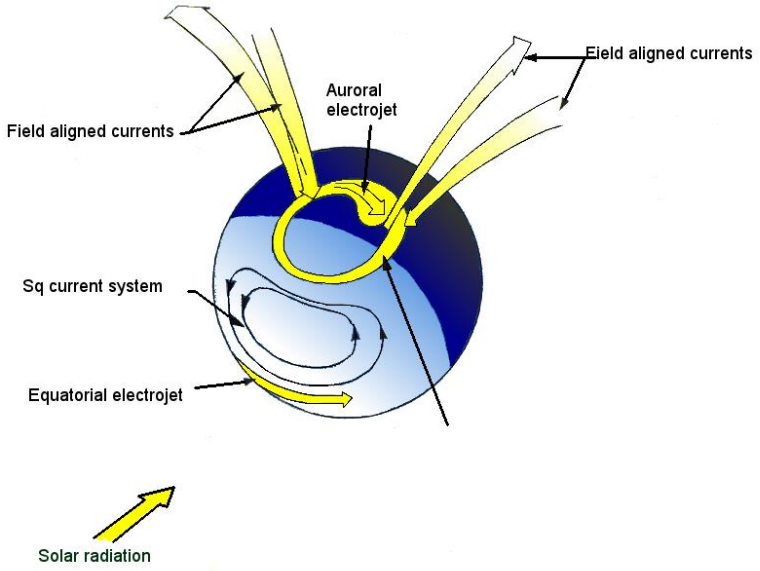

Figure 1: The ionospheric current system

EEJ – Equatorial electrojet. Along the geomagnetic equator in the ionosphere the Sq-dynamo generated eastward electric (E-)field and the horizontal (northward-oriented) geomagnetic field drives a vertical **E** x **B** drift separating the oppositely charged particles. The charge separation builds up an upward polarization E-field, an associated upward current, and also an eastward Hall-current that superimposes upon the primary eastward Sq-associated current. The result is an enhanced ionospheric conductivity and an enhanced current along the equator confined to a narrow range of latitude around ±3 ° peaking at 12 LT. The ground magnetic effect at the equator is 50-100 nT northward, but decreases rapidly away from the magnetic equator. EEJ has practically no ground effect poleward of 10° magnetic latitude.

SFE – a solar flare effect is a short-lived (< 10 minutes) modification of the ionospheric Sq current system related to increased ionization of the atmosphere from the EUV and X-ray emissions of a solar flare. Causes a rapid (over a few minutes) magnetic deviation/excursion in mid-latitudes of up to 50 nT. The mean mid-latitude amplitude is around 10-15 nT, the largest values occur near local noon (Curto et al., 1994). It is the first noticeable ground effect of an incoming solar storm, since the EUV and X-ray radiation reach the Earth with the speed of light, orders of magnitude faster than the speed of the solar wind that hardly ever surpasses 1500 km/s. SFE lists are available at http://www.obsebre.es/en/rapid.

Geomagnetic storms – are caused by the strong interaction of the solar wind, carrying an embedded solar magnetic field, with the Earth's magnetic field. Geomagnetic storms can be driven by fast solar wind flows originating from the solar coronal holes (so called co-rotating interactive regions, CIRs) or by interplanetary coronal mass ejections (ICMEs). The geoeffectivness of an ICME is related to the strength and duration of the southward-pointing component of the interplanetary magnetic field

(IMF). In the presence of a non-zero southward component, the oppositely-directed IMF and the geomagnetic field can merge (reconnection) opening geomagnetic field lines that are then convected tailward by the solar wind. Storm effects include an initial sudden storm commencement (**SSC**) and/or sudden impulse (**SI**) which are rapid (i.e. few minutes) rises in the magnetic field generated by the eastward magnetopause current associated with the motion of the magnetopause toward or away from the Earth as the solar wind pressure varies (Mayaud, 1975; Hafiz et al., 2013; Araki, 2014). The main phase of the geomagnetic storms is dominated by the effect of the ring current (RC) consisting of charged particles drifting around the Earth's magnetic equatorial region at a radial distance of about 5*R_e from the Earth's surface (where R_e is the Earth's radius). The RC is westward, producing a southward magnetic field on the ground that decreases the geomagnetic field globally. The effect of the RC decreases with magnetic latitude. The RC builds up gradually and can generate large magnetic fields (even over thousand nT, but typically a few hundred nT) over course of several days. The decay of the RC can take a week or longer (the so-called recovery phase).

The occurrence rate of storms has a strong solar cycle and a seasonal dependence (Mayaud, 1975), the latter peaking at equinoxes. The largest storms tend to occur near the sunspot maxima and during the declining phase of the solar cycle. The geomagnetic Dst (storm time disturbance) index characterizes the strength of the RC (available at http://wdc.kugi.kyoto-u.ac.jp/dst_realtime/presentmonth/index.html), while the Kp index (www.gfz-potsdam.de/en/kp-index/) characterizes the general level of the global geomagnetic activity independently of its actual source. SSC/SI lists are also available (http://www.obsebre.es/en/rapid).

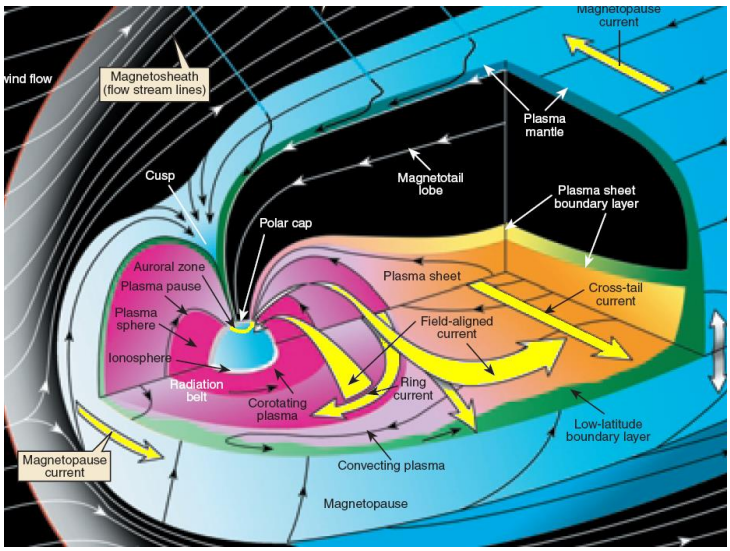

Figure 2: The magnetosphere with its primary current system

Magnetospheric Substorms – from time to time, as the stretched magnetic field lines in the magnetotail reconnect, the energy accumulated and stored in the tail is released and energized plasma particles are injected into the auroral region producing auroral brightening. These disturbances are called substorms and typically last a few hours. Substorms are much more frequent than geomagnetic storms and drive Field Aligned Currents which connect the magnetosphere into the ionosphere at high latitude. The high-latitude magnetic signatures of substorms are caused by the intensified ionospheric auroral electrojet current system that are formed between 60°-70° magnetic latitudes, but which can move equatorward towards 50° if the substorm is intense enough. They can generate magnetic fields of 1000s of nT close to the actual electrojet latitudes, decreasing

to 100s of nT at lower latitudes. The related disturbances at mid-latitudes are called positive bay disturbances, their typical amplitude is a few 10s of nT (Ritter and Lühr, 2008; Huang, 2009). The strength of the auroral electrojet/mid-latitude positive bay is characterized by the geomagnetic AE (or SME) index (Newell and Gjerloev, 2011) / MPB index (McPherron and Chu, 2017), expressed in nT and nT^2, respectively.

Wave phenomena

Faster magnetic variations, called geomagnetic pulsations can be almost always observed in the geomagnetic field during daytime. Their frequency covers the range from sub-mHz frequencies up to a few Hz. Pulsations were classified on a morphological basis in the 1960s, dividing them into two classes. The first is the class of the regular, continuous, sinusoid-like pulsations, termed Pc pulsations. The other is the class of impulsive, irregular pulsations, termed Pi pulsations. Both Pc and Pi pulsations are further divided according to their period. Geomagnetic pulsations are the ground manifestations of magnetospheric ultra-low frequency (ULF) waves. They can be modelled as magnetohydrodynamic (MHD) waves propagating in the cold (~1eV) magnetospheric plasma. In the cold plasma MHD two wave modes exist: the compressional mode that can propagate isotropically through magnetic field lines, and the shear-Alfvén mode with magnetic field-aligned propagation. Both propagate with the Alfvén speed that is roughly 1000 km/s in the inner magnetosphere. The two modes are always coupled in the highly inhomogeneous magnetosphere. While some of the magnetospheric ULF waves are driven by some external source (solar wind fluctuations, flow instabilities, etc.), others are generated locally by some resonance mechanisms. This happens frequently since the typical wave scales are comparable with the size of the magnetosphere. The most prominent manifestation of this latter type is the eigen-resonance of geomagnetic field lines in the shear-Alfvén mode, called the field line resonance (FLR). Compressional waves can also develop resonances e.g. cavity mode resonances, e.g. in the plasmasphere. Externally driven waves have typically low azimuthal wavenumber (*m*), so they can penetrate deep in the magnetosphere. By contrast, small-scale (high-*m*) waves are generated in the magnetosphere by some resonance mechanism through wave-particle interactions (drift or drift-bounce resonance). However, upon transmission through the ionosphere small-scale waves are smoothed out due to a spatial integration effect: the ground signal is the magnetic signature of ionospheric currents lowing at ~110 km altitude.

A recent, more detailed review of ULF waves can be found in Nakariakov et al. (2016). Here we focus on ground effects, the factors controlling their activity, as well as on their spatial and temporal distribution.

Pc4-5 waves (period: 45-150 s; 150-600 s)

An important way of energy transfer from the solar wind to the magnetosphere is via the Kelvin-Helmholtz instability (KHI). KHI appears where the flow shear between the solar wind and the magnetospheric plasma surpasses a certain threshold (Walker, 2015; Li et al., 2012, Nakariakov et al, 2016). As a result, small-scale fluctuations are grown into large-scale vortices at the boundary of the contacting media. This typically happens at the dawn and dusk flanks of the magnetosphere. These surface mode waves are coupled to evanescent mode waves in the magnetosphere. Related pulsations are in the Pc4-5 range - with the frequency depending on the flow parameters and geometrical factors. They are the strongest at high latitudes near local dawn and dusk. Since they

cannot penetrate deep into the magnetosphere, they are less important at mid- and low latitudes. KHI generated waves locally couple to FLRs at high latitudes, where their frequency matches the local FLR frequency. The FLR frequency primarily depends on the field line length and hence geomagnetic latitude. In general, the resonance frequency decreases with increasing latitude (except for near the plasmapause). Their typical amplitude at high/mid-latitudes is a few to a few 10s of nT.

Pc5 waves can also be driven directly by pressure variations intrinsic in the solar wind (Kepko and Spence, 2003; Viall et al., 2009; Nakariakov et al., 2016) through perturbing the size and shape of the whole magnetosphere (breathing mode). The resulting compressional waves can propagate deep in the magnetosphere (i.e. to lower latitudes), the penetration depth is controlled by the wave frequency and plasmaspheric density. Since this source is a dayside one, the related pulsations also appear on the dayside.

Solar wind pressure pulses (e.g. from the arrival of an ICME) on the magnetopause may also launch compressional waves into the magnetosphere. Due to the impulsive excitation these waves are broad band. In the magnetosphere they can also drive FLRs at different latitudes at wide a range of frequencies.

Poloidally polarised high-*m* (*m*>100) Pc4-5 waves driven by substorm injected energetic protons via drift- or drift-bounce resonance cannot be observed on the ground due to ionospheric spatial integration effects.

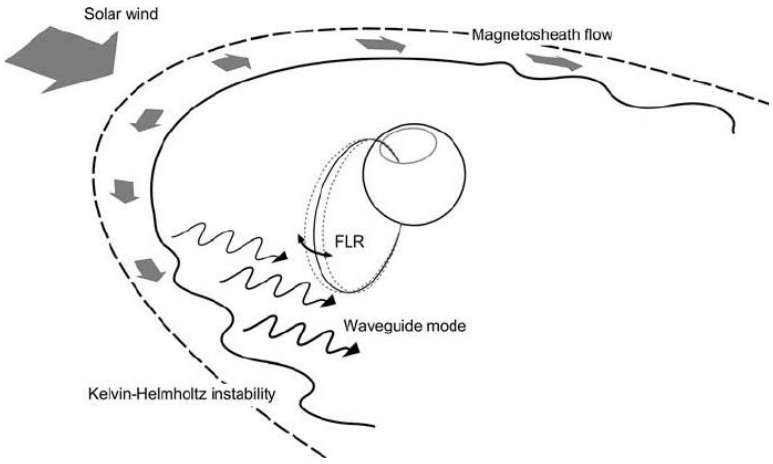

Figure 3: Generation of an FLR by a compressional wave

Pc3-4 waves (period: 10-45 s; 45-150 s)

Compressional waves observed in the dayside magnetosphere are generated in the terrestrial upstream foreshock by solar wind ions back-scattered from the bow shock standing 15 Re on average in front of the Earth toward the Sun (Heilig et al., 2010; 2007; Nakariakov et al., 2016). The resulting waves are called the upstream waves (UW). Due to their ion-cyclotron origin the frequency of the waves is proportional to the ambient magnetic field strength. In the magnetosphere and on the ground, they appear Doppler-shifted by the solar wind to frequencies in the Pc3-4 range ($f_{uw} \approx 6 \times B_{imf}$). Their amplitude is typically a few tenths or a few nT. At mid latitudes, where the FLR (10-100 mHz) frequency is in Pc3-4 the frequency range, they drive FLRs. As a result, there is a secondary ground activity peak at mid-latitudes. Both the compressional driver and the driven FLRs appear in

the same H-component on the ground, since the transverse FLR is rotated by 90° by the ionosphere (Hall-current effect), while the compressional waves are unaffected.

Pc2 waves (period: 5-10 s)

Although frequently found above the ionosphere, Pc2 waves are rarely observed on the ground, probably due to their small spatial scales (Yagova et al., 2015). Some of the Pc2 activity belongs the tail of the frequency distribution of other wave populations (high frequency upstream waves, or low frequency EMIC waves).

Pc1 waves (period: 0.2-5 s) – EMIC waves

Ground Pc1 waves are believed to be the manifestation of magnetospheric electromagnetic ion-cyclotron (EMIC) waves driven by energetic protons. Due to the localized generation mechanism, EMIC waves are also localized (~200-250 km at a few hundred km altitude) in space. Their latitudinal distribution peaks near the ionospheric footprint of the plasmapause, i.e. near 60° magnetic latitude (Park et al., 2013). However, since they can be ducted by the ionosphere, individual Pc1 waves can be observed with a larger extent on the ground (~1000 km). They occur dominantly on the night side (Bortnik et al., 2007; Park et al., 2013) and prefer quiet geomagnetic conditions (low Kp, low solar wind speed) (Park et al., 2013) following intense geomagnetic storms. Other authors reported on a high-latitude (L = 6-9) post-noon (LT= 12-16) maximum (Plyasova-Bakunina et al., 1996). Their amplitude in the topside ionosphere is typically below 0.5 nT but can reach a few nT occasionally (Park et al., 2013). Mid-latitude ground amplitudes are typically in the pT to tens of pT range (Nomura et al., 2011).

Pi2 waves (40-150 s) – substorm onset

Pi2 waves are associated with substorm onset, however, several Pi2 events can occur during a single substorm. They are believed to be generated by bursty plasma flows from the magnetotail or other impulsive night side sources (Keiling and Takahashi, 2011). Breaking-up fast plasma flows launch compressional waves earthward and drive fast mode cavity resonance confined to the plasmasphere. At the same time Alfvén waves travelling along the field lines reach high latitudes and perturb the electrojet. Pi2 waves are a typical night side (pre-midnight) phenomenon, although they can also propagate to the day side. Their typical amplitude at low- and mid-latitudes is sub-nT or a few nT, while in the auroral zone it sometimes exceeds 100 nT. A secondary maximum appears near the footprint of the plasmapause (on the average near magnetic latitude 60°) (Keiling and Takahashi, 2011; Kleimanova et al., 2014). The local time distribution (both occurrence and amplitude) peaks in the pre-midnight sector.

Pi1 waves (1-40 s)

Pi1B waves are a typical high-latitude, auroral phenomenon, another indicator of a substorm-onset. Pi1B waves are believed to be generated by the same or similar process as high-latitude Pi2s (Murphy et al., 2011; Rae et al., 2011). At geosynchronous orbit (at $6.6*R_e$ distance) in the tail they were observed as compressional waves, while deeper in the magnetosphere as dispersive shear-Alfvén waves (Lessard et al., 2006). Pi1B waves are broad band (up to ELF frequencies) pulsations

without any dominant frequency. They are believed to be responsible for the formation of the broad band electron population precipitating into the auroral ionosphere. Amplitudes are in the pT range.

ELF-VLF waves

There are two categories of electromagnetic waves in ELF-VLF frequency range (~3Hz-30kHz): natural and man-made waves (not considered here). The natural waves originate either from the ground weather phenomena or from the upper atmosphere. The various waves can be seen in Figure 4.

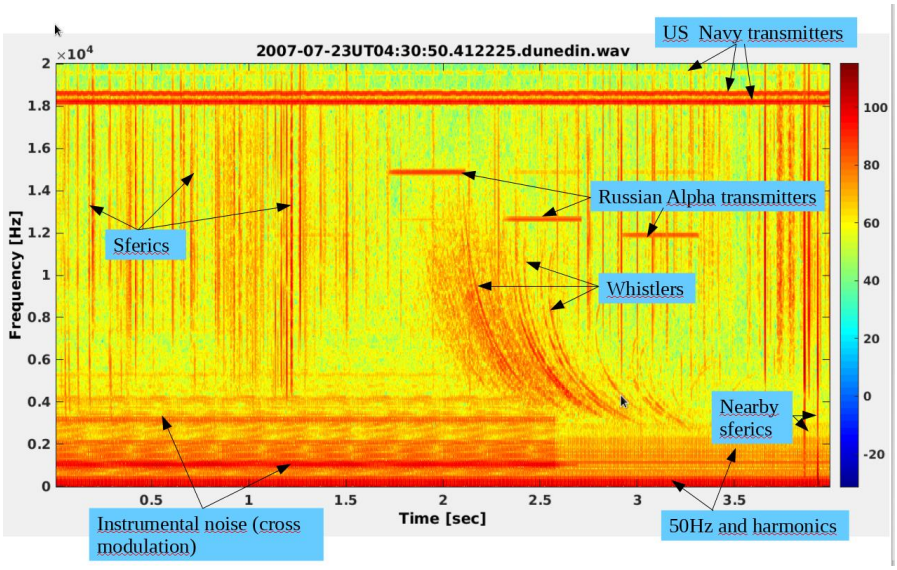

Figure 4: Spectrogram of exhibiting natural and man-made ELF-VLF waves

Schumann Resonances (SR)

SR are a global resonance in the Earth-Ionosphere cavity, excited by terrestrial lightning. The fundamental and strongest resonance is around 7.8Hz (this is not a constant frequency, changing due to variations in the height and shape of the bottom of the ionosphere. The second and third harmonics are at 14.3 and 20.8Hz, respectively.

The average amplitude of the fundamental resonance is around a few pT (Roldugin et al., 2006). SR are always present as the global lightning activity is a steady phenomenon, however, the amplitude of SR varies in time over the day and seasonally.

Sferics

Sferics are electromagnetic impulses generated by lightning discharges. The spectrum of a sferic at the source is white noise. However, the high frequency (> 100 kHz) part rapidly decays due to either propagation effect or strong attenuation in the atmosphere. At the same time, the energy in the ELF-VLF range can propagate for long distances as the attenuation is small (a few dB per 1000 km). Close to the lightning, the amplitude of the magnetic component is around 10 nT, while within a few hundred km, it decreases to ~1 nT and it is ~10 pT at several thousand km (Cummer, 1999, http://http://nova.stanford.edu/~vlf/palmer/palmer.htm#B2). Very close (few 100 m) lightnings can

produce over 10 μT change within 1 μs (Jerauld et al., 2009)! The typical rise time for more distant cloud-to-ground strokes is a 10-20 μs (Smith et al., 2001).

The occurrence of sferics at a specific location depends on the temporal variation of the activity of and distance from the source. The occurrence rate of lightning exhibits strong geographical, diurnal and seasonal variation, but the average global occurrence rate is fairly stable at around 100 strokes per second. The potentially dangerous sferics for CLIC are those generated by nearby lightning strikes. These can predicted based on local weather monitoring and forecast.

Whistlers

Whistlers are dispersed electromagnetic waves originated from sferics. Sferics can penetrate into the ionosphere and propagate along the magnetic field lines, where the propagation speed is strongly frequency dependent. The signal on the conjugate hemisphere penetrates through the ionosphere again and appears in the Earth-ionosphere waveguide as a dispersed signal (Helliwel, 1965). The amplitude of the signal depends on many factors, and it may reach ~1-2 nT at the magnetic equator (i.e. at the field line apex), generally weaker on the ground (10-100 pT).

The occurrence rate of whistlers near CERN is not measured yet, but one can extrapolate from the statistics collected at Tihany (Hungary) in the last two decades, at similar magnetic latitude (Lichtenberger et al., 2008). The occurrence rate of whistler at a ground location depends on the occurrence of the source at the conjugate region (Collier et al., 2010), the transparency of the ionosphere (diurnal dependence) and the presence of plasmaspheric ducts. The whistler activity at Tihany is around 50,000-100,000 traces/year. The average lightning activity at the conjugate region of CERN (~200km North-West of Cape Town, South Africa) is ~1/10 of those of the conjugate region of Tihany, thus we can assume 5,000-10,000 traces/year at CERN.

Choruses and hisses

Choruses are whistler mode waves generated at the magnetic equator, outside the plasmapause by the temperature anisotropy of energetic electrons. The generation process is triggered by natural VLF waves and governed by non-linear wave-particle interaction.

The origin of the hisses is still not completely understood, they may be generated by echoing whistler or obliquely propagating choruses after many reflections or by similar non-linear wave-particle interactions of those of choruses. The amplitudes of these waves are similar to those of whistlers (~1-2 nT at the magnetic equator, generally weaker on the ground, 10-100 pT).

The occurrence rate of choruses depends on the geomagnetic activity. The source electron population arrives from the magnetic reconnection region in the magnetotail, thus it is strongly connected to magnetic storms and substorms. Since choruses are generated outside the plasmapause, their occurrence at low magnetic latitude is negligible.

Though hisses occur inside the plasmasphere, their occurrence is mostly confined to the region close to the plasmapause, therefore the occurrence of hisses at CERN is also negligible (Golden et al., 2011).

VLF transmitters as globally observable man-made signals

Military and navigation VLF transmitters are all around the world, the most important ones are listed in Table 1.

Table 1. List of VLF transmitters (geographic coordinates, transmitted frequency, station code and location, modulation format, radiated power). The ones around Geneva are shaded.

LAT	LON	FREQ	SIGN	LOCATION	FORMAT	kW
50.07	135.6	11905Hz	RA1	Komsomolsk-na-Amur, Russia	CW	
45.40	38.18	12649Hz	RA2	Krasnodar, Russia	CW	
55.76	84.45	14881Hz	RA3	Novosibirsk, Russia	CW	
59.91	10.52	16400Hz	JXN	Kolsas, Norway (NATO)	FSK On/Off	45
8.47	77.40	18200Hz	VTX	Katabomman, India	FSK	
40.70	1.25	18300Hz	HWU	Rosnay, France	MSK	400
52.71	-3.07	19600Hz	GBZ	Anthorn, Great Britain (NATO)	FSK	30
-21.80	114.20	19800Hz	NWC	North West Cape, Australia (USA)	MSK	1000
40.88	9.68	20270Hz	ICV	Isola di Tavolara, Italy (NATO)	MSK	20
25.03	111.67	20600Hz	3SA	Changde, China	FSK	
39.60	103.33	20600Hz	3SB	Datong, China	FSK	
40.70	1.25	20900Hz	HWU	Rosnay, France	MSK	400
20.40	-158.20	21400Hz	NPM	Lualualei, Hawaii, USA	MSK	424
40.70	1.25	21750Hz	HWV	Le Blanc, France (NATO)	MSK	200
52.40	-1.20	22100Hz	GQD	Anthorn, Great Britain (NATO)	FSK	
32.04	130.81	22200Hz	JJI	Ebino, Japan	FSK	200
53.10	7.60	23400Hz	DHO	Rhauderfehn, Germany (DHO)	FSK	800
44.65	-67.30	24000Hz	NAA	Cutler, Maine, USA	MSK	1000
48.20	-121.90	24800Hz	NLK	Jim Creek, Washington, USA	MSK	192
46.35	-98.33	25200Hz	NLM	LaMoure, North Dakota, USA	MSK	
37.43	27.55	26700Hz	TBB	Bafa, Turkey	MSK	
65.00	-18.00	37500Hz	NRK	Grindavik, Iceland (USA)	MSK	
18.00	-67.00	40750Hz	NAU	Aguado, Puerto Rico (USA)	MSK	100
38.00	13.50	45900Hz	NSC	Sicily, Italy (USA)	MSK	

The transmitted power varies between 20 kW-1 MW, but the efficacy of them is either low or very low (0.00001-20 %). The near-field magnetic field strength of NPM (424 kW) measured in the transmitter building near the feed line varied between 140-18,000 nT (!) [Guy and Chou, 1982], but decreases rapidly. The magnetic field strength observed at 7 km distance was 3 nT. The attenuation of the signal strongly depends on LT and on the conductivity of the ground between the transmitter and the receiver and it is the same as for sferics (see above). As the locations of the VLF transmitter around CERN are known, the propagation and the signal attenuation can be modelled or - this may be easier – can be measured at CERN.

Inductive and skin effects

GIC – Geomagnetically Induced Currents arise from the interaction of the time-varying magnetic field with the (slightly) conductive ground. Electric fields (called the geoelectric field) are created whose strength strongly depends on the local geology. Areas of poorly conductive rock (e.g. granite, basalt, metamorphic rock) can attain very high fields for several minutes (> 1 V/km) during the passage of the auroral electrojets (at high latitudes) for example (Ngwira et al, 2013, Fujii et al, 2015). Large gradients in conductivity within the surface geology can act as channels for electrical current flow. If

the geoelectric fields encounter a low resistance manmade structure, such as a pipeline or a grounding point in a high-voltage electrical transmission power line, then currents can flow easily through these systems potentially causing damage to electronics or the transformer cores (e.g. Beggan et al, 2013).

We note that inductive effect of lightning could also be a source of very strong stray magnetic fields.

The electromagnetic waves penetrate into the ground (skin effect) to a depth corresponding to the excitation frequency of the source. The skin depth can be estimated as:

$$\delta = 1/\sqrt{\pi f \mu \sigma}$$

where μ is the magnetic susceptibility, σ is the conductivity of the material, and f is the wave frequency. The average skin depth in the ELF-VLF waves ranges from 100 m (24 kHz) to 5 km (10 Hz). The critical parameter is the rocks' conductivity: the lower the conductivity, the larger the skin depth. ULF waves penetrate even deeper (few 10s to few 100s km), hence most of the surface waves appear with negligible attenuation in a tunnel at 100 m depth.

Conclusion

CLIC beam stability is sensitive only to the dynamic field contributions, the rate of change, rather than the field strength. The sensitivity threshold is around 1 nT/s. Table 2 summarizes the magnetic effect of the various phenomena, their mean amplitude, duration, typical time scales (or frequency range) and also the daily, monthly and yearly extremes. The table is based on the cited literature and all available magnetic data (North component) recorded at a 1 Hz cadence at Tihany between 2007-2017, as well as the observations made by its local VLF receiver. Considering both the possible amplitude extremes and the time scales, the 1 nT/s threshold is exceeded only rarely at mid-latitudes. Only the infrequent geomagnetic storms (27 of the storm events during the 11 years), especially their SSC (13 of the 27 storms), some of the substorm-related Pi2 pulsations (13 events) and most frequently the EM pulses/waves launched by close lightning strokes can reach that level at geomagnetic mid-latitudes. The most rapid (> 2 nT/s) SSC rise rates were 8 nT/s (Sep 12, 2014), 5-6 nT/s (Jan 24, 2012) and 3-4 nT/s (Jun 22, 2015). Apart from an exceptional Pi2 event exceeding 5 nT/s rate of change, all the rest of the geomagnetic disturbances associated with rapid field change rates remained below the 2 nT/s level. At the same time, as observed close to the source, the rise time of sferics is 1-10 μs, and the rate of change can surpass 10 μT per 1 μs. Hence, the highest risk in the ELF-VLF band is posed by nearby lightning discharges. Geomagnetic storms are potentially dangerous (especially in regions with low ground conductivity) through their associated GICs, especially if the currents flow close to the experiment, producing large magnetic field locally.

It is also important to recall, that the above values are only valid for mid-latitudes (~45° magnetic latitude). The most severe geomagnetic conditions take place in general at higher latitudes under and near the auroral oval. At high latitudes, the disturbance level associated with various phenomena, especially substorms can easily be an order of magnitude higher or even greater than at mid-latitudes. Other types of disturbances dominate at low and equatorial latitudes. From geomagnetic point of view, the latitude of CERN is close to the optimum choice.

Table 2. Summarizing the main characteristics of the considered phenomena at CERN's geomagnetic latitude (based on data recorded at Tihany between 2007-2017)

Phenomenon	Occurrence (local time)	Duration	Frequency (Hz) content (or period)	Average magnitude	Once in a day	Once in a month	Once in a year	Predictability/model
Sq variation	regular diurnal variation	daytime	24 h and its harmonics	15–80 nT	15-80 nT	n/a	n/a	yes
Solar flare effect*	daytime, rare	15-20 min (rise time: 3-6 min)	few to 10 minutes	10–15 nT	n/a	n/a	n/a	no
Geomagnetic storms*	infrequent	days	minutes to days	< 100 nT	n/a	~130 nT (daily)	~270 nT (daily)	yes
SSC*	infrequent	2-10 min	minutes	20-30 nT	n/a	20-30 nT	~ 60 nT	yes
Geomagnetic substorms*	infrequent	1-4 hours	minutes to hours	10–20 nT	n/a	n/a	> 50 nT	no
Pc5 waves	regular, near dawn and dusk	several hours	150–600 s	450 pT	> 1.6 nT	> 6.5 nT	> 12.5 nT	no
Pc4 waves	regular, daytime	several hours	45–150 s	120 pT	> 800 pT	> 2.1 nT	> 3.8 nT	no
Pc3 waves	regular, daytime	several hours	10–45 s	50 pT	> 700 pT	> 1.6 nT	> 2.5 nT	yes
FLRs	regular, daytime	daytime	20–25 s	1 nT	> 700 pT	> 1.6 nT	> 2.5 nT	yes
Pi2 waves	infrequent, pre-midnight	several minutes	40–150 s	few nT	< 1 nT	< 5 nT	< 10 nT	no
Pc2 waves	rare	n/a	5–10 s	12 pT	> 100 pT	> 600 pT	> 1.3 nT	no
Pi1 waves	infrequent, pre-midnight	several minutes	1–40 s	few pT	?	?	?	no
Pc1 waves	infrequent night time	several minutes	0.2–5 s	few pT	?	?	?	no
Schumann resonances	regular, all day	continuous	~ 8 Hz and harmonics	~1 pT	?	?	?	yes
VLF hiss	disturbed periods		VLF	10–100 pT	?	?	?	
VLF chorus	infrequent	n/a	VLF	negligible	n/a	n/a	n/a	no
Lightnings triggered sferics	global thunderstorm activity	few ms (rise time for close strokes: 1-10s μs)	broad band impulse	1–10 nT nT	n/a	n/a	> 1 μT	yes
Lightning triggered whistlers	geomagnetically conjugate thunderstorms	few seconds	ELF–VLF	10–100 pT	n/a	n/a	~ 1 nT	yes
GIC*	generated by geomagnetic storms and substorms	hours	minutes to hours	0–100 mV/km	n/a	n/a	~250 mV/km	no

* there is a strong dependence also on the 11-year solar activity cycle and the terrestrial seasons

References

Araki, T. (2014), Historically largest geomagnetic sudden commencement (SC) since 1868, Earth, Planets and Space, 66, 164, doi.org/10.1186/s40623-014-0164-0.

Beggan, C., Beamish, D., Kelly, G.S., Richards, A., and A. W. P. Thomson (2013), Prediction of Geomagnetically Induced Currents in the United Kingdom's National Grid, *Space Weather*, 11, doi: 10.1002/swe.20065

Bortnik, J., J. W. Cutler, C. Dunson, and T. E. Bleier (2007), An automatic wave detection algorithm applied to Pc1 pulsations, *J. Geophys. Res.*, 112, A04204, doi:10.1029/2006JA011900.

Collier, A. B., Bremner, S., Lichtenberger, J., Downs, J. R., Rodger, C. J., Steinbach, P., and McDowell, G. (2010) Global lightning distribution and whistlers observed at Dunedin, New Zealand, *Ann. Geophys*., 28, 499-513, https://doi.org/10.5194/angeo-28-499-2010.

Cummer, S.A. (1999): Lightning and Ionospheric Remote Sensing Using VLF/ELF Radio Atmospherics, PhD thesis, Stanford University.

Curto, J.J., Ch. Amory-Mazaudier, J.M. Torta, M. Menvielle (1994), Solar flare effects at Ebre: Regular and reversed solar flare effects, statistical analysis (1953 to 1985), a global case study and a model of elliptical ionospheric currents, *J. Geophys. Res.*, 99 (A3), 3945-3954.

Fujii, I., Ookawa, T., Nagamachi, S. et al. (2015), The characteristics of geoelectric fields at Kakioka, Kanoya, and Memambetsu inferred from voltage measurements during 2000 to 2011, *Earth Planet Space*, 67, 62, doi:10.1186/s40623-015-0241-z

Golden, D. I., M. Spasojevic, and U. S. Inan (2011), Determination of solar cycle variations of mid-latitude ELF/VLF chorus and hiss via automated signal detection, *J. Geophys. Res.*, doi:10.1029/2010JA016193.

Guy AW, Chou CK (1982): Hazard Analysis: ‘‘Low Frequency Through Medium Frequency Range.’’ Brooks Air Force Base, TX: U.S. Air Force School of Aerospace Medicine.

Hafez, A.G., E. Ghamry, H. Yayama, K. Yumoto (2013), Systematic examination of the geomagnetic storm sudden commencement using multi resolution analysis, *Adv. Space Res.*, 51, 39-49, doi.org/10.1016/j.asr.2012.07.035.

Helliwell, R. A. (1965), Whistlers and Related Ionospheric Phenomena, Stanford Univ. Press, Stanford, Calif.

Heilig B., P. R. Sutcliffe (2016), Coherence and phase structure of compressional ULF waves at low-Earth-orbit observed by the Swarm satellites, *Geophysical Research Letters* 43, 945-951, doi:10.1002/2015GL067199.

Heilig B., H. Lühr, M. Rother (2007), Comprehensive study of ULF upstream waves observed in the topside ionosphere by CHAMP and on the ground. *Annales Geophysicae*, *25*, 737-754.

Heilig, B., S. Lotz, J., Verő, P. Sutcliffe, J. Reda, K. Pajunpää, and T. Raita (2010), Empirically modelled Pc3 activity based on solar wind parameters. *Annales Geophysicae*, 28, 1703–1722.

Heilig B., P. R. Sutcliffe, D. C. Ndiitwani, A. Collier (2013), Statistical study of geomagnetic field line resonances observed by CHAMP and on the ground*, Journal of Geophysical Research Space Physics*, *118*, 1934-1947, doi: 10.1002/jgra.50215.

Huang, C.-S. (2009), Eastward electric field enhancement and geomagnetic positive bay in the dayside low-latitude ionosphere caused by magnetospheric substorms during sawtooth events, *Geophys. Res. Lett*., 36, L18102, doi: 10.1029/2009GL040287.

Jerauld, J. E., M. A. Uman, V. A. Rakov, K. J. Rambo, D. M. Jordan, and G. H. Schnetzer (2009), Measured electric and magnetic fields from an unusual cloud-to-ground lightning flash containing two positive strokes followed by four negative strokes, *J. Geophys. Res.*, 114, D19115, doi: 10.1029/2008JD011660.

Keiling, A. and Takahashi, K. (2011), Review of Pi2 Models, *Space Sci*. *Rev*. 161, 63. doi:10.1007/s11214-011-9818-4.

Kepko, L., H.E. Spence (2003), Observations of discrete, global magnetospheric oscillations directly driven by solar wind density variations. *Journal of Geophysical Research Space Physics*, 108, 1257, doi:10.1029/2002JA009676.

Kleimenova, N.G., Zelinsky, N.R. & Kotikov, A.L. (2014), Analysis of latitudinal distribution of Pi2 geomagnetic pulsations using the generalized variance method, *Geomagn*. *Aeron*., 54, 308, doi:10.1134/S0016793214030098.

Lessard, M. R., E. J. Lund, S. L. Jones, R. L. Arnoldy, J. L. Posch, M. J. Engebretson, and K. Hayashi (2006), Nature of Pi1B pulsations as inferred from ground and satellite observations, *Geophys. Res. Lett.*, 33, L14108, doi:10.1029/2006GL026411.

Li, W.Y., X.C. Guo, C. Wang (2012), Spatial distribution of Kelvin-Helmholtz instability at low-latitude boundary layer under different solar wind speed conditions. *J. Geophysi. Res.*, 117, 8230, doi:10.1029/2012JA017780.

Lichtenberger, J., C. Ferencz, L. Bodnar, D. Hamar, and P. Steinbach (2008), Automatic Whistler Detector and Analyzer system: Automatic Whistler Detector, *J. Geophys. Res.*, 113, A12201, doi: 10.1029/2008JA013467.

Lotz, S.I., B. Heilig, and P.R. Sutcliffe (2015), A solar wind driven empirical model of Pc3 wave activity at a mid-latitude location, *Annales Geophysicae*, *33* (2015), 225-234, doi:10.5194/angeo-33-225-2015.

Mayaud, P. N. (1975), Analysis of storm sudden commencements for the years 1868–1967, *J. Geophys. Res.*, 80(1), 111–122, doi: 10.1029/JA080i001p00111.

McPherron, R.L. and Chu, X. (2017), *Space Sci. Rev.*, 206, 91-122, doi:10.1007/s11214-016-0316-6.

Murphy, K. R., I. J. Rae, I. R. Mann, and D. K. Milling (2011), On the nature of ULF wave power during nightside auroral activations and substorms: 1. Spatial distribution, *J. Geophys. Res.*, 116, A00I21, doi:10.1029/2010JA015757.

Nakariakov, V., V.A. Pilipenko, B. Heilig, P. Jelínek, M. Karlický, D.Y. Klimushkin, D.Y. Kolotkov, D.-H. Lee, G. Nisticò, T. Van Doorsselaere, G. Verth, I.V. Zimovets (2016), Magnetohydrodynamic Oscillations in the Solar Corona and Ultra-Low Frequency Oscillations in the Earth's Magnetosphere: Towards Consolidated Understanding. *Space Science Reviews* 200, 75-203, 2016, doi:10.1007/s11214-015-0233-0

Newell, P. T., and J. W. Gjerloev (2011), Evaluation of SuperMAG auroral electrojet indices as indicators of substorms and auroral power*, J. Geophys. Res.*, 116, A12211, doi: 10.1029/2011JA016779.

Ngwira, C. M., A. Pulkkinen, F. D. Wilder, and G. Crowley (2013), Extended study of extreme geoelectric field event scenarios for geomagnetically induced current applications, *Space Weather*, 11, 121–131, doi: 10.1002/swe.20021.

Nomura, R., K. Shiokawa, V. Pilipenko, and B. Shevtsov (2011), Frequency-dependent polarization characteristics of Pc1 geomagnetic pulsations observed by multipoint ground stations at low latitudes, *J. Geophys. Res.*, 116, A01204, doi:10.1029/2010JA015684.

Park, J., Lühr, H., and Rauberg (2013), J.: Global characteristics of Pc1 magnetic pulsations during solar cycle 23 deduced from CHAMP data, *Ann. Geophys.*, 31, 1507-1520, doi:10.5194/angeo-31-1507-2013.

Pilipenko, V.A., B. Heilig (2016), ULF waves and transients in the topside ionosphere, A. Keiling, D.H. Lee, V. Nakariakov (eds.), *Low-frequency waves in space plasmas* (AGU Geophysical Monograph Series 216), Wiley, 2016, pp 15-29, doi: 10.1002/9781119055006.

Plyasova-Bakounina, T. A., J. Kangas, K. Mursula, O. A. Molchanov, and A. W. Green (1996), Pc 1-2 and Pc 4-5 pulsations observed at a network of high-latitude stations, *J. Geophys. Res*., 101, 10965-10973.

Rae, I. J., K. R. Murphy, C. E. J. Watt, and I. R. Mann (2011), On the nature of ULF wave power during nightside auroral activations and substorms: 2. Temporal evolution, *J. Geophys. Res*., 116, A00I22, doi:10.1029/2010JA015762.

Ritter, P. and Lühr, H.: Near-Earth magnetic signature of magnetospheric substorms and an improved substorm current model, *Ann. Geophys*., 26, 2781-2793, https://doi.org/10.5194/angeo-26-2781-2008, 2008.

Roldugin, V. C., A. N. Vasiljev, and A. A. Ostapenko (2006), Comparison of the Schumann resonance parameters in horizontal magnetic and electric fields according to observations on the Kola Peninsula, *Radio Sci.*, 41, RS2S07, doi:10.1029/2006RS003475

Smith, D. A., K. B. Eack, J. Harlin, M. J. Heavner, A. R. Jacobson, R. S. Massey, X. M. Shao, and K. C. Wiens (2002), The Los Alamos Sferic Array: A research tool for lightning investigations, *J. Geophys. Res.*, 107(D13), doi: 10.1029/2001JD000502.

Viall, N.M., L. Kepko, H.E. Spence (2009), Relative occurrence rates and connection of discrete frequency oscillations in the solar wind density and dayside magnetosphere. *J. Geophys. Res.*, 1201, doi:10.1029/2008JA013334

Walker, A.D.M. (1981), The Kelvin-Helmholtz instability in the low-latitude boundary layer. *Planetary and Space Science* 29, 1119–1133. doi:10.1016/0032-0633(81)90011-8

Walker, A.D.M. (2005), *MHD Waves in Geospace* (Institute of Physics Publishing, London)

Yagova, N. V., B. Heilig, and E. N. Fedorov, (2015) Pc2-3 geomagnetic pulsations on the ground in the magnetosphere, and in the ionosphere. MM100, CHAMP and THEMIS observations, *Annales Geophysicae*, 33, 117-128, doi:10.5194/angeo-33-117-2015